CHEMISTRY & CHEMICAL TECHNOLOGY

Vol. 6, No. 2, 2012 Chemistry

Oleg Figovsky[1], Dmitry Pashin[2], Zufar Khalitov[2] and Diana Valeeva[2]

THE STRUCTURE AND DIFFRACTION BY CHIRAL NANOTUBES OF ARBITRARY COMPOSITION

[1]International Nanotechnology Research Center "Polymate", Migdal Haemek 23100, Israel
[2]Kazan State Technical University, 10, K. Marx str., Kazan, Tatarstan 420111, Russia
pashin@addnano.ru

Received: September 26, 2011 / Revised: October 02, 2011 / Accepted: December 09, 2011

Abstract. The quantitative theory of diffraction by separate chiral nanotubes of arbitrary chemical composition is offered. The pseudoorthogonality effect and dependence of diffraction on the azimuthal ordering are considered. The calculated diffraction patterns for the case of electron microdiffraction by separate chrysotile nanotubes are adduced.

Keywords: nanotube, chiral nanotube, chirality indexes.

1. Introduction

Diffraction by the chiral lattice was considered by E. Whittaker in the middle of the last century in the approach to close packing of layers [1]. More detailed consideration of the problem [2] shows that close-packed chiral lattice is impossible. After first investigation of carbon nanotubes the description of atoms arrangement and the diffraction theory [3, 4] without using the concepts of unit cell and applicable only to this structure and to similar ones were developed. However researches of the last decade have resulted in significant expansion of the nanotubes nomenclature and in the necessity of formulation of more general mathematical apparatus for diffraction simulation. The purpose of this research is the analysis of diffraction by single-wall and multi-wall chiral nanotubes of arbitrary chemical composition in view of the features of radial packing of their layers.

The peculiarity of the considered model of nanotube is the assumption of the tendency of its layers to inheritance of mutual orientation [2]. Then cylindrical coordinates of atoms of the multiwall cylindrical chiral nanotube of arbitrary composition, which layers have longitudinal linear Δz_m (m = 0, 1, 2, … – number of a layer) and azimuthal angular ε_m shifts and close chiral angles ε_{cm} [2] concerning a general origin, can be written down as:

$$\begin{cases} r_{mj} = \dfrac{w_m}{2p} + x_j \\ j_{mnnj} = \dfrac{2p}{w_m^2}\left[bp_m\left(bn + y_j\right) - as_m\left(an + z_j\right)\right] + e_m = a_{1m}n - b_{1m}n + g_{1mj} \\ z_{mnnj} = \dfrac{1}{w_m}\left[as_m\left(bn + y_j\right) + bp_m\left(an + z_j\right)\right] + \Delta z_m = a_{2m}n + b_{2m}n + g_{2mj} + \Delta z_m \end{cases} \quad (1)$$

where chiral indexes of the m-th layer (p_m, s_m), expressed in numbers of Bravais cells along the turn of structure and on the step of helix, respectively, are determined as nearest integers from:

$$p_m = \frac{2p r_m}{b}\cos e_c, \qquad s_m = \frac{2p r_m}{a}\sin e_c, \qquad r_m = r_{m-1} + d$$

and $$a_{1m} = \frac{2pb^2 p_m}{w_m^2}, \qquad b_{1m} = \frac{2pa^2 s_m}{w_m^2}, \qquad a_{2m} = \frac{abs_m}{w_m}, \qquad b_{2m} = \frac{abp_m}{w_m}$$

$$g_{1mj} = 2p\,\frac{bp_m y_j - as_m z_j}{w_m^2} + e_m, \quad g_{2mj} = \frac{as_m y_j + bp_m z_j}{w_m}, \quad w_m = \sqrt{(as_m)^2 + (bp_m)^2} \quad (2)$$

where n and v – numbers of unit cells in directions of measurement of lattice parameters a and b, respectively; d – thickness of a layer; j – number of atom in an unit cell; x_j, y_j, z_j – linear coordinates of atom in an unit cell in a radial direction and in directions of measurement of lattice parameters b and a, respectively.

The rectangular Bravais cell in a layer is chosen in such a manner that parameter a is measured in the direction closest to nanotube's axis and parameter b – in the direction closest to a circle of the cylinder. Value ρ_0 is determined from

$$2\pi r_0 = \sqrt{(as_0)^2 + (bp_0)^2}$$

where (p_0, s_0) – chiral indexes of an internal layer, the chiral angle of which is equal to ε_c. The same values are considered as the chiral indexes of multiwall chiral nanotube. Hence, the chiral angles of nanotube's layers are given by the expressions:

$$\mathrm{tg}\varepsilon_c = \frac{as_0}{bp_0}, \qquad \mathrm{tg}\varepsilon_{cm} = \frac{as_m}{bp_m}$$

The modeling profiles of diffraction are calculated for the case of electron microdiffraction by a separate chrysotile nanotube. The correction multipliers (absorption, etc) on this stage of development were not taken into account.

2. Amplitude of Diffraction

Entering in reciprocal space the cylindrical coordinate system {R, φ^*, z^*} the diffraction amplitude by structure (1) can be written down as:

$$A(R, \varphi^*, z^*) = \sum_{n=0}^{N-1}\sum_{m=0}^{M-1}\sum_{n=0}^{p_m-1}\sum_{j} f_j \cdot$$

$$\exp\left\{2\pi i\left[Rr_{mj}\cos(\varphi_{mnnj} - \varphi^*) + z^* z_{mnnj}\right]\right\} =$$

$$= \sum_m \sum_j F_{mj}(z^*) \sum_n \exp(2\pi i z^* a_{2m} n) \cdot$$

$$\sum_n \exp(2\pi i z^* b_{2m} n) \exp\left[2\pi i R r_{mj}\cos(\varphi_{mnnj} - \varphi^*)\right] \quad (3)$$

where

$$F_{mj}(z^*) = f_j \exp(2\pi i z^* g_{2mj}) \exp(2\pi i z^* \Delta z_m) \quad (4)$$

M – number of cylindrical layers in nanotube; N – number of site turns along the cylinder's axis; f_j –scattering function of j-th atom. Let us expand the last exponent in (3) into a series of cylindrical waves corresponding to:

$$\exp(ia\cos\gamma) = J_0(a) + 2\sum_{q=1}^{\infty} i^q \cos(q\gamma) J_q(a)$$

Then $A(R, \varphi^*, z^*) = A_0(R, z^*) + A_D(R, \varphi^*, z^*)$,

where $A_0(R, z^*) = \sum_m \sum_j F_{mj}(z^*) J_0(2\pi R r_{mj})$ (5)

$$\sum_n \exp(2\pi i z^* a_{2m} n) \sum_n \exp(2\pi i z^* b_{2m} n) \cdot$$

$$\cdot A_1(R, \varphi^*, z^*) = 2\sum_m \sum_j F_{mj}(z^*) \cdot$$

$$\cdot \sum_n \exp(2\pi i z^* a_{2m} n) \sum_n \exp(2\pi i z^* b_{2m} n) \cdot$$

$$\cdot \sum_{q=1}^{\infty} i^q \cos\left[q(\varphi_{mnnj} - \varphi^*)\right] J_q(2\pi R r_{mj}) \quad (6)$$

Let us consider addendum (5). The sums over n and v have character δ-functions, therefore the sum over n has appreciable values only at:

$$z^* p b_{2m} = hp \quad \Rightarrow \quad z^* = \frac{hw_m}{abp_m},$$

$$h = 0; \pm 1; \pm 2; \ldots \quad (7)$$

and the sum over v – at

$$z^* p a_{2m} = kp \quad \Rightarrow \quad z^* = \frac{kw_m}{abs_m},$$

$$k = 0; \pm 1; \pm 2; \ldots \quad (8)$$

Comparing (7) and (8), we obtain: $hs_m = kp_m$, that generally gives the unique decision: $h = 0$, $k = 0$. From this, in turn, follows $z^* = 0$ – an equation of layer plane (or, in crossing with Ewald sphere, of a layer line), on which all reflexes, corresponding to amplitude (5), are located. Thus, this addendum describes the amplitude of strong [5] reflexes of a zero layer line (the number of a layer line or plane coincides with the value of index h):

$$A_S^{00l}(R) = N\sum_j f_j \sum_{m=0}^{M-1} p_m J_0(2\pi R r_{mj}) \quad (9)$$

where the index "S" means strong reflexes.

Let us consider amplitude (6) as:

$$A_1(R, \varphi^*, z^*) = \sum_{m,j} F_{mj}(z^*) \sum_{q=1}^{\infty} i^q J_q(2\pi R r_{mj}) S_{qmj} \quad (10)$$

where

$$S_{qmj} = 2\sum_n \exp(2\pi i z^* a_{2m} n) \cdot$$

$$\cdot \sum_n \exp(2\pi i z^* b_{2m} n) \cos[q(\varphi_{mnnj} - \varphi^*)] =$$

$$= A_{qm} \exp[iq(\gamma_{1mj} - \varphi^*)] + B_{qm} \exp[-iq(\gamma_{1mj} - \varphi^*)] \quad (11)$$

$$A_{qm} = \sum_{v=0}^{p_m-1} \exp\left[i\left(2p\, z^* a_{2m} + q a_{1m}\right)v\right] \cdot$$
$$\cdot \sum_{n=0}^{N-1} \exp\left[i\left(2p\, z^* b_{2m} - q b_{1m}\right)n\right]$$
$$B_{qm} = \sum_{v=0}^{p_m-1} \exp\left[i\left(2p\, z^* a_{2m} - q a_{1m}\right)v\right] \cdot$$
$$\cdot \sum_{n=0}^{N-1} \exp\left[i\left(2p\, z^* b_{2m} + q b_{1m}\right)n\right] \qquad (12)$$

In the second column of Table 1 the conditions of extremum of the sums, which are included in (12), are given. The products of these sums will give combinations of conditions of extremenesses, being the systems of equations for determination of the values of z^* and q (the third column of the Table 1, h, k - integers), at which the maxima of every m-th addendum of amplitude (10) are reached. This allows choosing the members of a series which make the basic contribution to intensity of scattering.

Because of the symmetry of reciprocal space it is enough to investigate distribution of intensity in one of its halves, for example, with $z^* \geq 0$. As in the majority of practically important cases $bp_m > as_m$, from the third column of the Table it follows that only reflexes with $h \geq 0$ will be considered. The exception will be the diffuse ($k \neq 0$) reflexes with $h = 0$, which will be split in pairs with $z^* > 0$ and $z^* < 0$.

The index of a series $q > 0$ by definition, therefore from the third column of Table 1 it follows that the multiplier A_{qm} describes diffuse reflexes with $k > 0$, and B_{qm} – with $k < 0$. The last multiplier gives also strong ($k = 0$) reflexes with $h > 0$, as the strong reflexes with $h = 0$ are described by amplitude (9). In fourth column of the Table the maximal values of multipliers are given.

Pseudoorthogonal reflexes, as well as in case of circular nanotube [5], are formed by the main maxima of Bessel functions, which are included in expression for strong reflexes. Let us consider positions of pseudoorthogonal reflexes of the layer lines with $h > 0$. From (2) and definition of radius of a chiral layer (1) it follows that:

$$w_m = \sqrt{(as_m)^2 + (bp_m)^2} = 2p\, r_m$$

Substituting this in z_m^* from the Table 1 at $k = 0$ and taking into account expression for p_m from (2) we obtain:

$$z_m^* = \frac{h}{a}\cos e_{cm} \qquad (13)$$

On the other hand, the main maxima of Bessel functions are near to points appropriating to equality of their argument to the index. Then from (10) and the third line of the third column of Table 1 at $k = 0$:

$$2pRr_m = hs_m \Rightarrow R_m^0 = \frac{h}{a}\sin e_{cm} \qquad (14)$$

where x_j was neglected and expression (2) for the chiral index s_m was taken into account. From comparison of expressions (13) and (14) it follows that the maxima of m-th addendums of amplitude (10), corresponding to pseudoorthogonal reflex, displace along arch of a circle of radius h/a with the centre in the origin of reciprocal space when the chiral angle changes.

Table 1

Conditions of a maximum of multipliers which are included in function S_{qmj}

Multiplier	Conditions of a maximum	Value of variables	Value of multiplier
A_{qm}	$(2pz^* b_{2m} - q b_{1m})/2 = hp$ $(2pz^* a_{2m} + q a_{1m})/2 = kp$	$z_m^* = \frac{hb^2 p_m + ka^2 s_m}{abw_m}$, $q = kp_m - hs_m$	Np_m
B_{qm}	$(2pz^* b_{2m} + q b_{1m})/2 = hp$ $(2pz^* a_{2m} - q a_{1m})/2 = kp$	$z_m^* = \frac{hb^2 p_m + ka^2 s_m}{abw_m}$, $q = -kp_m + hs_m$	Np_m

3. Diffraction by a Singlewall Chiral Nanotube

In this case in the sum over m in expressions (9) and (10) there remains the only addendum corresponding to $m = 0$, and in expressions (1), (2) and (4) it is necessary to put $\varepsilon_m = 0$, $\Delta z_m = 0$. Then, according to (9), the intensity of the singlewall chiral nanotube zero layer line strong reflexes will look like:

$$I_S(R) = N^2 p_0^2 \left[\sum_j f_j J_0\left(2pRr_{0j}\right)\right]^2$$

From Table 1 it follows that h-th layer lines of strong and diffuse reflexes of the singlewall chiral nanotube will have coordinates

$$z_h^* = \frac{h}{a}\cdot\frac{bp_0}{w_0} = \frac{h}{a}\cos e_c, \text{and}$$

$$z_{hk}^* = \frac{h}{a}\cdot\frac{bp_0}{w_0} + \frac{k}{b}\cdot\frac{as_0}{w_0} = \frac{h}{a}\cos e_c + \frac{k}{b}\sin e_c \qquad (15)$$

correspondingly. Function (11) and amplitude (10) become:

$$S_{q0j} = Np_0 \exp\left[i\left(kp_0 - hs_0\right)\left(g_{10j} - j^*\right)\right]$$

$$A_1\left(R, j^*\right) = i^q Np_0 \exp\left[-i\left(kp_0 - hs_0\right)j^*\right]\cdot$$

$$\cdot\sum_j F_{0j}\left(z_{hk}^*\right)\exp\left[i\left(kp_0 - hs_0\right)g_{10j}\right]J_q\left(2p\,R\,r_{0j}\right)$$

$$A_1\left(R, j^*\right) = i^q Np_0 \exp\left[-i\left(kp_0 - hs_0\right)j^*\right]\cdot$$

$$\cdot\sum_j F_{0j}\left(z_{hk}^*\right)\exp\left[i\left(kp_0 - hs_0\right)g_{10j}\right]J_q\left(2p\,R\,r_{0j}\right)$$

where
$$q = \begin{cases} kp_0 - hs_0 & , \quad k > 0 \\ -kp_0 + hs_0 & , \quad k < 0 \\ hs_0 & , \quad k = 0 \end{cases} \qquad (16)$$

and the weak overlapping of Bessel functions is taken into account too. The corresponding intensity

$$I_1(R) = N^2 p_0^2 \left|\sum_j f_j \exp\left[2pi\left(h\frac{z_j}{a} + k\frac{y_j}{b}\right)\right]\cdot\right.$$

$$\left.\cdot J_q\left(2pRr_{0j}\right)\right|^2 \qquad (17)$$

has no angular dependence.

It is possible to estimate from (15) and (17) positions of the main maxima of diffuse reflexes equating argument of the Bessel function to its index and omitting addendum x_j:

$$\begin{aligned} hk: &\quad R_{hk} \approx \frac{kp_0 - hs_0}{w_0}, \quad z_{hk}^* = \frac{hp_0b^2 + ks_0a^2}{abw_0}, \\ h\bar{k}: &\quad R_{h\bar{k}} \approx \frac{kp_0 + hs_0}{w_0}, \quad z_{h\bar{k}}^* = \frac{hp_0b^2 - ks_0a^2}{abw_0}, \end{aligned} \qquad (18)$$

where the index k is taken in absolute value.

From (18) it is seen that the diffuse reflex with $k > 0$ has place above the layer plane $z^* = (h/a)\cos\varepsilon_c$ and is closer to a point $R = 0$, and the reflex with $k < 0$ is lower and farther. The module of a reciprocal space vector of the diffuse reflex main maximum $R_{hk}^* = \sqrt{R_{hk}^2 + z_{hk}^{*2}} = \frac{1}{ab}\sqrt{(ka)^2 + (hb)^2}$. It means that the splitting of diffuse reflexes occurs along the arch of a circle with centre at the origin of reciprocal space when the chiral indexes change. From (18) it also follows that the linear and angular distances between the main maxima of diffuse reflexes with opposite sign of index k can be written down as:

$$\Delta_{hk}^* = \frac{2s_0}{b}\cdot\frac{\sqrt{(ka)^2 + (hb)^2}}{\sqrt{(bp_0)^2 + (as_0)^2}}, e_{hk} \approx \frac{\Delta_{hk}^*}{R_{hk}^*} = \frac{2as_0}{\sqrt{(bp_0)^2 + (as_0)^2}}$$

When $s_0 = 1$, $a = 0.53$ nm and $bp_0 \approx 25$ nm (approximately corresponds to chrysotile) this gives $\varepsilon_{hk} \approx 2.5^0$, which is in good agreement with the experimental results [6].

The choice of q from the expression (16) allows obtaining the profiles of intensity of any reflexes of the singlewall chiral nanotube from (17). The strong reflexes are presented only by reflexes $h0$ (Fig. 1).

The examples of profiles of diffuse reflexes with $h = 1$ and various values of index k and second chiral index s_0 are shown in Fig. 2. The profiles in Figs. 1 and 2 are combined on one diagram conditionally, as, according to (15), they have different coordinates z^*.

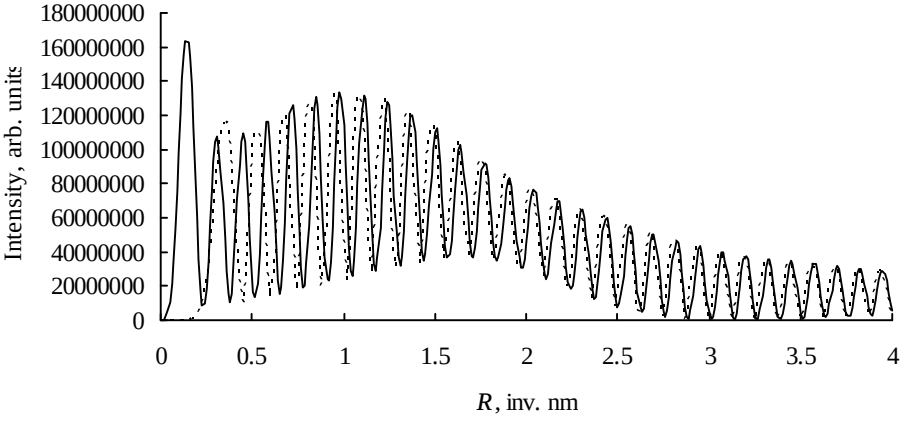

Fig. 1. Reflexes 20 of the chrysotile singlewall chiral nanotubes with chiral indexes (27,1) (solid) and (27,3) (dotted)

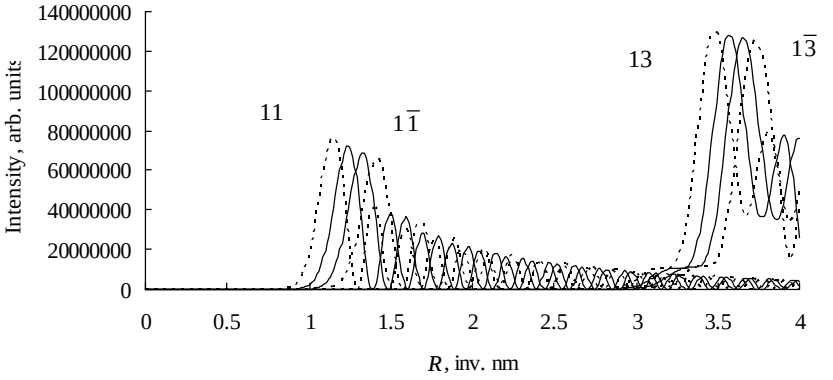

Fig. 2. Pairs of diffuse reflexes $1k\,-1\bar{k}$ from chrysotile singlewall chiral nanotubes with chiral indexes (27,1) (solid) and (27,3) (dotted)

4. Diffraction by a Multiwall Chiral Nanotube

The positions of the maxima of addendums of scattering amplitude by the multiwall chiral nanotube, according to the third column of the Table 1, depend on a layer number *m*. Therefore for modeling diffraction it is necessary to calculate the distribution of intensity in some area of change of values *R* and *z**, covering the whole area of existence of maxima of scattering amplitude addendums. For this purpose it is necessary to present amplitudes of scattering in another form.

The purpose of the previous analysis was finding the conditions of simultaneous extremeness of the sums over *n* and *v*, which gave values of coordinates of maxima *z** and conditions for the members of series over *q*. Now the purpose is finding the maxima of the pointed pair products at any values *z**, close to the values given in the third column of Table 1.

Calculation of the sums, included in multipliers (12), gives:

$$A_{qm} = C^{+}_{qm} D^{-}_{qm}\,,\; B_{qm} = C^{-}_{qm} D^{+}_{qm} \qquad (19)$$

Where

$$C^{\pm}_{qm} = \frac{\sin\left[p_m \left(pz^{*} a_{2m} \pm \frac{q a_{1m}}{2} \right) \right]}{\sin\left(pz^{*} a_{2m} \pm \frac{q a_{1m}}{2} \right)} \cdot$$

$$\exp\left[i(p_m - 1)\left(pz^{*} a_{2m} \pm \frac{q a_{1m}}{2} \right) \right]$$

$$D^{\pm}_{qm} = \frac{\sin\left[N\left(pz^{*} b_{2m} \pm \frac{q b_{1m}}{2} \right) \right]}{\sin\left(pz^{*} b_{2m} \pm \frac{q b_{1m}}{2} \right)} \cdot$$

$$\cdot \exp\left[i(N-1)\left(pz^{*} b_{2m} \pm \frac{q b_{1m}}{2} \right) \right] \qquad (20)$$

At arbitrary values of variable *z** the values (20) will be maximal at values *q*, given in the Table 2, where in the fourth column the maximal values of multipliers are also given. It means that as a first approximation for every *m*-th addendum it is possible to choose two members of a series, which give the greatest contribution to amplitude of a reflex. Thus, each of the products (19) will enter into amplitude of a reflex two times: first time will be maximal the first multiplier of product, second time – the second.

It is obvious that it is necessary to round off the values of *q* from Table 2 during the calculations. Parameter *t*, arising from a condition of a maximum of expressions (20), is integer too. The comparison of the data of Tables 1 and 2 at *z**, corresponding to the third column of Table 1, gives conditions for this parameter, that were given in third column of Table 2.

As it was already noted, the factor A_{qm} in (11) corresponds to diffuse reflexes with $k > 0$, and factor B_{qm} – to diffuse reflexes with $k < 0$. Then, according to (19), in the case of diffuse reflexes with $k > 0$ with arbitrary coordinate *z** from multiwall chiral nanotube the amplitude (10) may be presented as:

$$A_D^{hk0}\left(R, j^{*}, z^{*}\right) = \sum_{m,j} F_{mj}(z^{*}) \left\{ i^{q_1} p_m D^{-}_{q_1 m} \cdot \right.$$

$$\cdot \exp\left[i q_1 \left(g_{1mj} - j^{*} \right) \right] J_{q_1}\left(2pRr_{mj} \right) +$$

$$\left. + i^{q_4} C^{+}_{q_4 m} N \exp\left[i q_4 \left(g_{1mj} - j^{*} \right) \right] J_{q_4}\left(2pRr_{mj} \right) \right\} \qquad (21)$$

and in the case $k < 0$:

$$A_D^{h\bar{k}0}\left(R, j^{*}, z^{*}\right) = \sum_{m,j} F_{mj}(z^{*}) \left\{ i^{q_2} p_m D^{+}_{q_2 m} \cdot \right.$$

$$\cdot \exp\left[-iq_2\left(g_{1mj}-j^*\right)\right]J_{q_2}\left(2pRr_{mj}\right)+$$

$$+i^{q_3}C^{-}_{q_3m}N\exp\left[-iq_3\left(g_{1mj}-j^*\right)\right]J_{q_3}\left(2pRr_{mj}\right)\Big\} \quad (22)$$

where the index "*D*" means diffuse reflexes.

In Fig. 3 the examples of calculated distributions of intensity corresponding to amplitude (21) of diffuse reflex 130 from multiwall monoclinic ($\Delta z_m = m\Delta z$, $\Delta z = -a/13$) nanotubes with various second chiral indexes are shown in coordinates {*R*, φ^*}. The distributions have *kg*-multiple symmetry, the availability of the reciprocal lattice's centre of symmetry in a case *kg* - odd is provided by the similar distribution of a reflex $\bar{1}30$ (at opposite value of z^*), turned on 180^o [7].

Table 2

Conditions of extremeness of expressions (20)

Multiplier	Values of *q*	Conditions for *t*	Value of multiplier
C^{+}_{qm}	$q_1=-\frac{2p}{a_{1m}}\left(z^*a_{2m}-t\right)=-\frac{as_mw_m}{bp_m}z^*+k\frac{w_m^2}{b^2p_m}$	$t=k$	p_m
C^{-}_{qm}	$q_2=\frac{2p}{a_{1m}}\left(z^*a_{2m}-t\right)=\frac{as_mw_m}{bp_m}z^*-k\frac{w_m^2}{b^2p_m}$	$t=k$	p_m
D^{+}_{qm}	$q_3=-\frac{2p}{b_{1m}}\left(z^*b_{2m}-t\right)=-\frac{bp_mw_m}{as_m}z^*+h\frac{w_m^2}{a^2s_m}$	$t=h$	N
D^{-}_{qm}	$q_4=\frac{2p}{b_{1m}}\left(z^*b_{2m}-t\right)=\frac{bp_mw_m}{as_m}z^*-h\frac{w_m^2}{a^2s_m}$	$t=h$	N

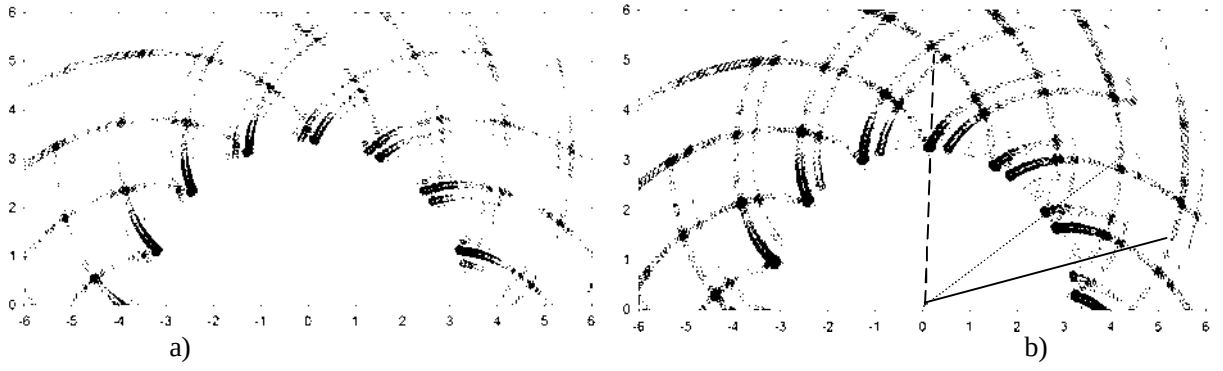

Fig. 3. Distributions of intensity of a reflex 130 from chrysotile multiwall monoclinic nanotubes in a plane {*R*, φ^*} with chiral indexes: (27,1) (a) and (27,4) (b)

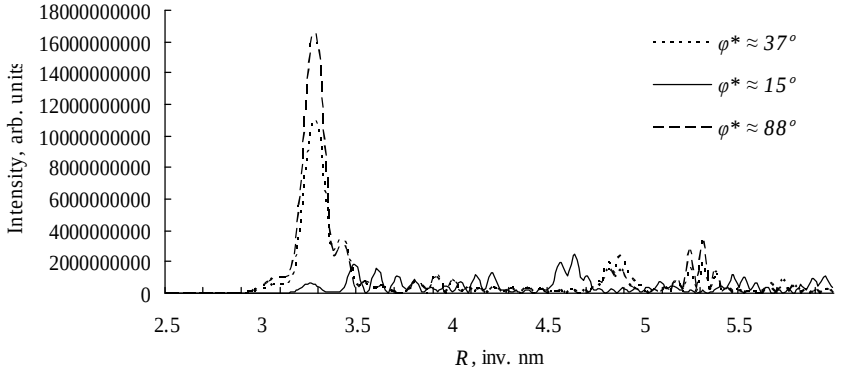

Fig. 4. A reflex 130 from chrysotile's chiral monoclinic nanotube (27,4) with various angles φ^*

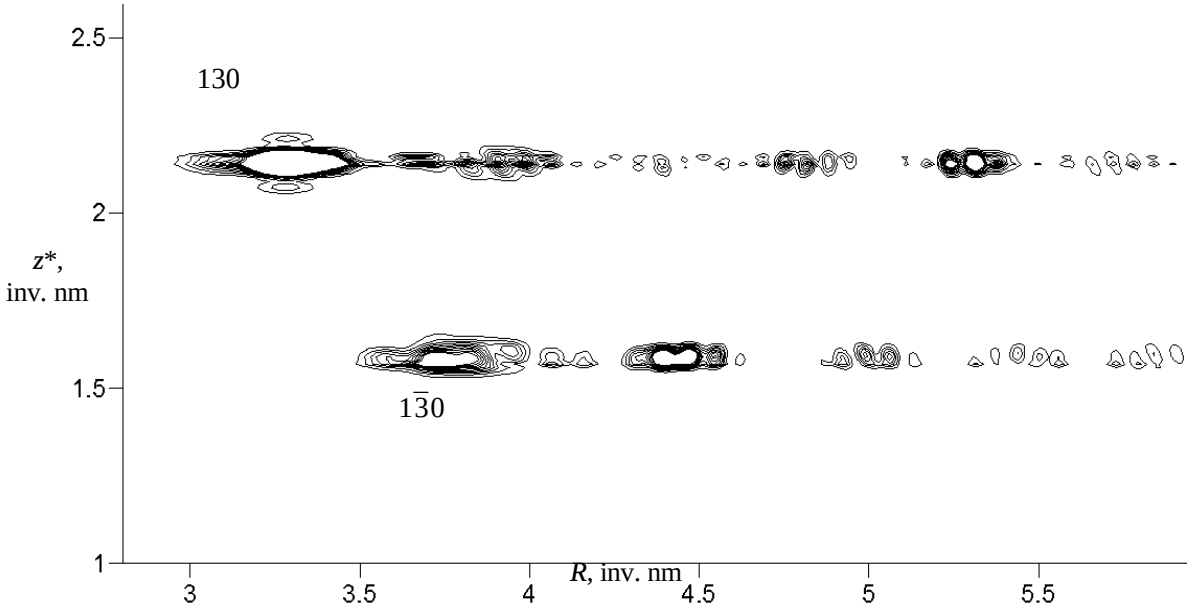

Fig. 5. A doublet 130-1$\bar{3}$0 from chrysotile chiral monoclinic nanotube (27,4) in a plane $\{R, z^*\}$ at $\varphi^* = 5^o$

The examples of calculation of diffraction profiles lengthways the layer lines, marked in Fig. 3b by direct lines, are shown in Fig. 4 by the lines of the same type. The distinctions in profiles mean that the experimental patterns of electron microdiffraction by separate chiral nanotube will depend essentially on their azimuthal orientation on an electron beam. Hence, in spite of the fact that the modern experimental techniques allow to register patterns, showed in Fig. 3 only for $z^* = 0$ it is necessary to simulate the distributions of all reflexes in a plane $\{R, \varphi^*\}$ for correct interpretation of experimental data.

Fig. 5 shows the example of calculation of intensity distribution for a chrysotile chiral monoclinic nanotube's doublet 130-1$\bar{3}$0 in a plane $\{R, z^*\}$, that corresponds to a usual experimental electron microdiffraction pattern (the intensity levels from 0 up to 10 % through 1 % are shown only). On distribution the main maxima of diffuse reflexes and oscillations of intensity in the area of their tails, which are similar to oscillations in Fig. 4 and having same origin, are clearly visible. Thus, though every addendum of diffraction amplitude, appropriate to a layer of nanotube, has its own value of a extremum point z_m^*, the summation of these addendums results in forming diffuse reflex with quite certain coordinate z^*.

Determination of a chiral angle by the main maxima gives value $\varepsilon_c \approx 5.4^o$, while its calculation at $p_0 = 27$, $s_0 = 4$ and parameters of a chrysotile lattice gives $\varepsilon_c \approx 4.9^o$. The reason is, apparently, the variations of chiral angles of separate layers owing to a rounding off.

The strong reflexes result from general expression (10) under condition of $k = 0$. An index of a series $q \geq 1$ by definition, that in application to the Table 2 means, that its second line corresponds to $z^* < 0$. Being limited by the half-space with $z^* > 0$ we shall take into account only values C_{qm}^- and D_{qm}^+, that is value B_{qm} and addendums, connected with it in (11). The taken into account members of a series are:

$$q_2 = \frac{as_m w_m}{bp_m} z^*$$

$$\text{and } q_3 = -\frac{bp_m w_m}{as_m} z^* + h\frac{w_m^2}{a^2 s_m} \qquad (23)$$

with a rounding off. It is necessary to remember that here $h \geq 1$, as the strong reflexes of a zero layer plane are already given by expression (9). It is obvious that the required amplitude is described by expression (22), where parameter q_2 should be taken from (23):

$$A_S^{h0l}\left(R, j^*, z^*\right) = \sum_{m,j} F_{mj}(z^*)\left\{i^{q_2} p_m D_{q_2 m}^+ \cdot \right.$$

$$\cdot \exp\left[-iq_2\left(g_{1mj} - j^*\right)\right] J_{q_2}\left(2pRr_{mj}\right) +$$

$$\left. + i^{q_3} C_{q_3 m}^- N \exp\left[-iq_3\left(g_{1mj} - j^*\right)\right] J_{q_3}\left(2pRr_{mj}\right)\right\} \qquad (24)$$

Calculations of intensity (Fig. 6) appropriate to amplitude (24) in a plane $\{R, \varphi^*\}$ show that the strong reflexes with $h > 0$ from chiral nanotubes, as against the circular ones, have spiral character. In this case the step of a spiral in reciprocal space is much less than in the case of

diffuse reflexes (Fig. 3), but strongly depends on the second chiral index s_0. Hence, in case of strong reflexes with $h > 0$ the experimental patterns of electron microdiffraction by separate chiral nanotube will depend on its azimuthal orientation about its own axis (Fig. 7).

In Fig. 8 the examples of calculation of second layer line strong reflexes profiles from chrysotile monoclinic nanotubes with various chiral indexes are shown. The appreciable displacement of reflexes with $l \neq 0$ to the beginning of a layer line with increasing of the second chiral index is observed. Thus the reflex 200, overlapped with a pseudoorthogonal reflex 20, is displaced in an opposite direction, and its intensity quickly decreases. This effect proves to be true by calculations of intensity distribution in a plane $\{R, z^*\}$ in the area of a second layer line (Fig. 9).

During research of chrysotile nanotube's oriented polycrystalline preparations by the method of X-ray scanning of reciprocal space [8] there were samples whose reflex $20\bar{1}$ had a considerable low-angle tail [7]. It can be explained by spiral character of strong reflexes from chiral nanotubes and their dependence on the chiral indexes.

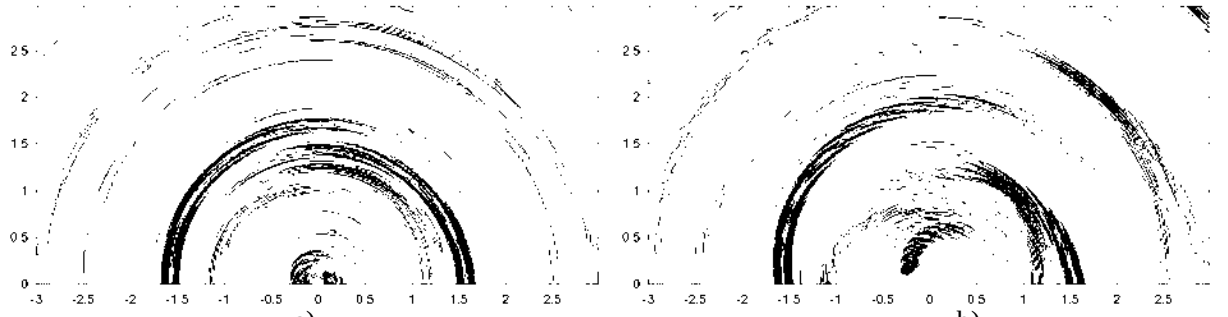

Fig. 6. Distributions of intensity of strong reflexes with $h = 2$ from chrysotile chiral monoclinic nanotubes in a plane $\{R, \varphi^*\}$ with chiral indexes: (27,1) (a) and (27,3) (b)

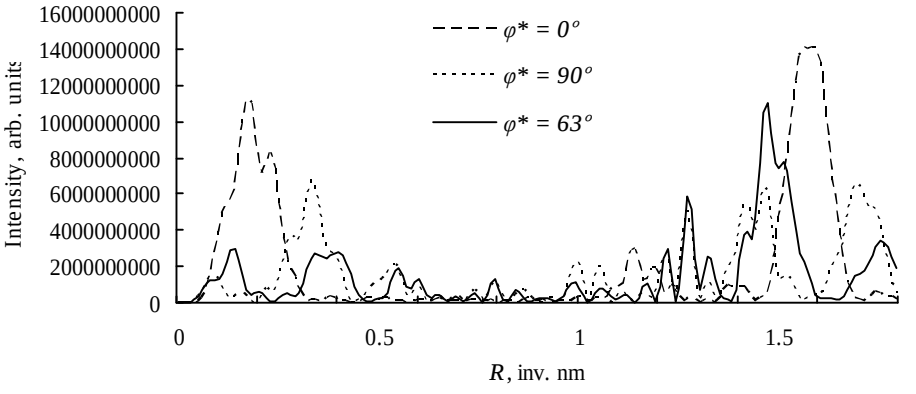

Fig. 7. Profiles of strong reflexes of a second layer line from chrysotile's chiral nanotube (27,1) at various φ^*

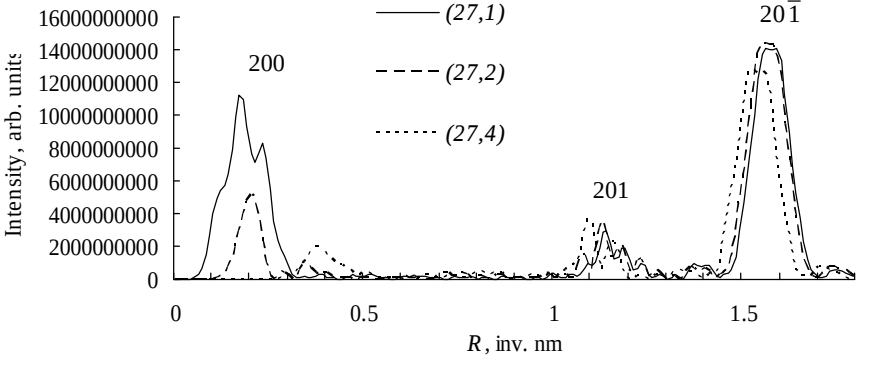

Fig. 8. Profiles of second layer line strong reflexes from monoclinic chrysotile nanotube with various chiral indexes at $\varphi^* = 0$

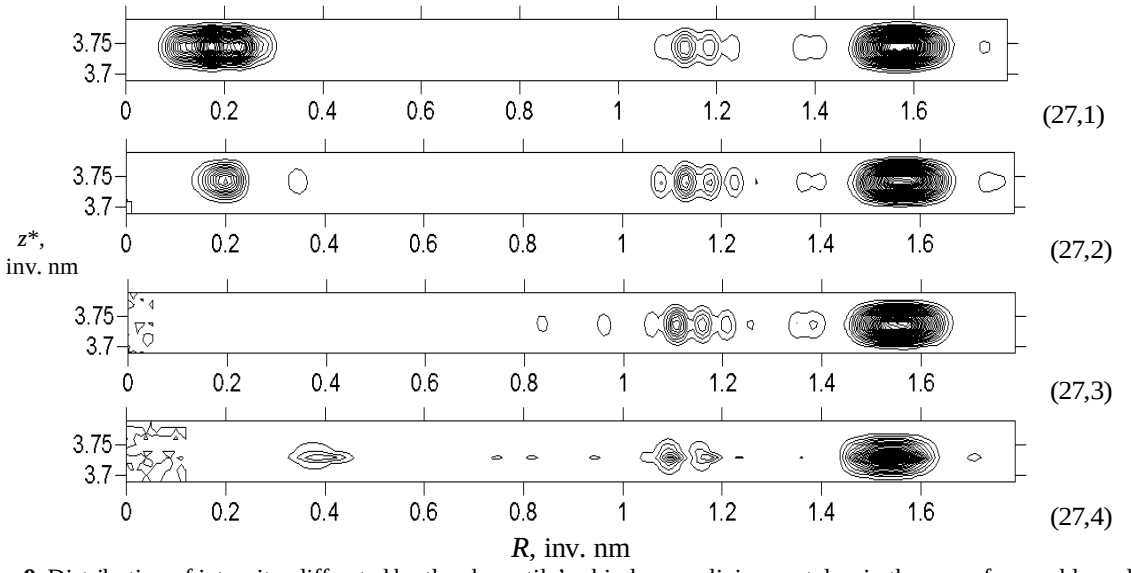

Fig. 9. Distribution of intensity, diffracted by the chrysotile's chiral monoclinic nanotubes in the area of second layer line on a plane $\{R, z^*\}$ at $\varphi^* = 0$ (the chiral indexes of nanotubes on the right are given)

5. Diffraction by a Multiwall Azimuthal Disordered Chiral Nanotube (Whittaker's Model)

In the model of multiwall cylindrical nanotube, proposed by Whittaker, initial angular phases ε_m, included in γ_{1mj}, have random character [9]. Then in intensity of diffuse reflexes with $k > 0$, corresponding to amplitude (21),

$$I_D^{hk0}\left(R, j^*, z^*\right) = \sum_{m,m'} \sum_{j,j'} \left\{ G_{mj1} \cdot \right.$$

$$\left. \cdot \exp\left[iq_1\left(g_{1mj} - j^*\right)\right] + G_{mj4} \exp\left[iq_4\left(g_{1mj} - j^*\right)\right] \right\} \cdot$$

$$\cdot \left\{ G^*_{m'j'1} \exp\left[-iq'_1\left(g_{1m'j'} - j^*\right)\right] + \right.$$

$$\left. + G^*_{m'j'4} \exp\left[-iq'_4\left(g_{1m'j'} - j^*\right)\right] \right\} =$$

$$= \sum_{m,m'} \sum_{j,j'} \left\{ G_{mj1} G^*_{m'j'1} \exp\left[iq_1\left(g_{1mj} - j^*\right)\right] \right.$$

$$\left. \exp\left[-iq'_1\left(g_{1m'j'} - j^*\right)\right] + \right.$$

$$+ G_{mj1} G^*_{m'j'4} \exp\left[iq_1\left(g_{1mj} - j^*\right)\right] \exp\left[-iq'_4\left(g_{1m'j'} - j^*\right)\right] +$$

$$+ G_{mj4} G^*_{m'j'1} \exp\left[iq_4\left(g_{1mj} - j^*\right)\right] \exp\left[-iq'_1\left(g_{1m'j'} - j^*\right)\right] +$$

$$\left. + G_{mj4} G^*_{m'j'4} \exp\left[iq_4\left(g_{1mj} - j^*\right)\right] \exp\left[-iq'_4\left(g_{1m'j'} - j^*\right)\right] \right\}$$

where
$$\begin{cases} G_{mj1} = F_{mj}(z^*) i^{q_1} p_m D^-_{q_1 m} J_{q_1}\left(2pRr_{mj}\right) \\ G_{mj4} = F_{mj}(z^*) i^{q_4} N C^+_{q_4 m} J_{q_4}\left(2pRr_{mj}\right) \end{cases} \quad (25)$$

will remain only addendums, appropriate $m' = m$:

$$I_D^{hk0}\left(R, j^*, z^*\right) = \sum_m \sum_{j,j'} \left\{ G_{mj1} G^*_{mj'} \cdot \right.$$

$$\left. \cdot \exp\left[iq_1\left(d_{1mj} - j^*\right)\right] \exp\left[-iq_1\left(d_{1mj'} - j^*\right)\right] + \right.$$

$$\left. + G_{mj4} G^*_{mj'4} \exp\left[iq_4\left(d_{1mj} - j^*\right)\right] \exp\left[-iq_4\left(d_{1mj'} - j^*\right)\right] \right\} =$$

$$= \sum_m \left[\left| \sum_j G_{mj1} \exp\left(iq_1 d_{1mj}\right) \right|^2 + \left| \sum_j G_{mj4} \exp\left(iq_4 d_{1mj}\right) \right|^2 \right],$$

$$d_{1mj} = g_{1mj} - e_m = 2p \frac{bp_m y_j - as_m z_j}{w_m^2}$$

Substituting (4) and (25), we obtain finally:

$$I_D^{hk0}\left(R, z^*\right) = \sum_m p_m^2 \left| D^-_{q_1 m} \right|^2 \left| \sum_j f_j \cdot \right.$$

$$\left. \cdot \exp\left(2piz^* g_{2mj}\right) \exp\left(iq_1 d_{1mj}\right) J_{q_1}\left(2pRr_{mj}\right) \right|^2 +$$

$$+ N^2 \sum_m \left| C^+_{q_4 m} \right|^2 \left| \sum_j f_j \exp\left(2piz^* g_{2mj}\right) \exp\left(iq_4 d_{1mj}\right) J_{q_4}\left(2pRr_{mj}\right) \right|^2$$

In case $k < 0$, that is in case of intensity appropriate amplitude (22), operating similarly, we obtain:

$$I_D^{h\bar{k}0}\left(R, z^*\right) = \sum_m p_m^2 \left| D^+_{q_2 m} \right|^2 \left| \sum_j f_j \cdot \right.$$

$$\left. \cdot \exp\left(2piz^* g_{2mj}\right) \exp\left(-iq_2 d_{1mj}\right) J_{q_2}\left(2pRr_{mj}\right) \right|^2 +$$

$$+ N^2 \sum_m \left| C^-_{q_3 m} \right|^2 \left| \sum_j f_j \exp\left(2piz^* g_{2mj}\right) \exp\left(-iq_3 d_{1mj}\right) J_{q_3}\left(2pRr_{mj}\right) \right|^2 \quad (26)$$

The same expression at $k = 0$, that is at q_2 and q_3 from (23), describes the strong reflexes from multiwall chiral nanotube of the Whittaker's model too. This means that in this case in the sum over layers (over m) which generates series of strong reflexes only positive values are summarized and arising of the sharp and separate maxima of intensity is impossible. Hence, in the Whittaker's model the strong reflexes take place only on a zero layer line according to (9). On the other layer lines the "strong" analogue of expression (26) gives only the background component with a pseudoorthogonal maximum. As follows from the carried out analysis, in the Whittaker's case the angular dependence of multiwall chiral nanotube's reflexes is also absent.

In Fig. 10 the examples of calculated profiles of the strong reflexes of chrysotile nanotube's second layer line in the Whittaker's case with various second chiral indexes s_0 are given. The profiles represent continuous distribution of intensity beginning from reflex 200. The intensity oscillations in the areas 0.6-0.7 nm^{-1} and 1.3-1.4 nm^{-1} are not associated with any strong reflex of chrysotile. It is necessary to notice that the authors did not face similar diffraction patterns either during researches or the scientific literature. Nevertheless, the presence of an appreciable level of background in the area of layer lines of oriented polycrystalline chrysotile samples allows assuming a possibility of existence of such nanotubes.

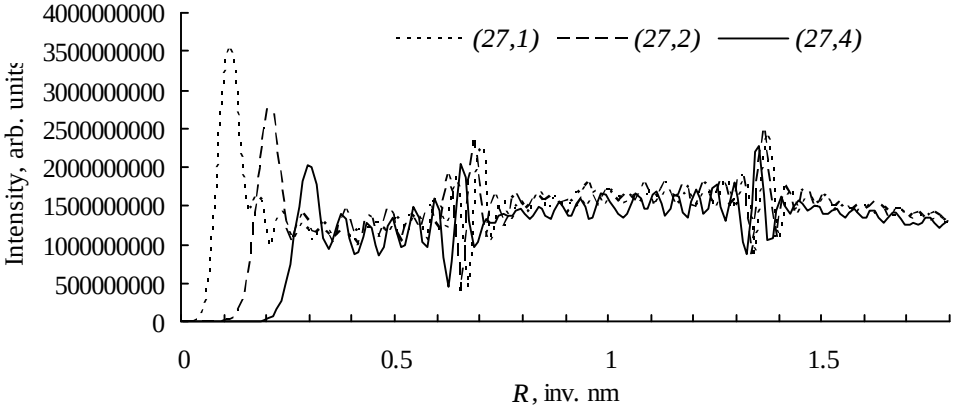

Fig. 10. Profiles of strong reflexes of chrysotile nanotube's second layer line of Whittaker's model with various chiral indexes

6. Conclusions

The carried out analysis and the modeling calculations allow making a set of conclusions. First, diffraction by chiral nanotubes, in comparison with the circular ones [5], represents a more complex phenomenon and gives more difficult diffraction patterns for interpretation. Dependence of the displacement of coordinates of layer lines and reflexes of chiral nanotube's microdiffraction pattern on chiral indexes makes the determination of lattice parameters rather complicated. It is obvious that the correct determinations are possible only on the basis of analysis of distributions of reflexes intensities in a plane $\{R, \varphi^*\}$ with taking into account the azimuthal orientation of nanotube about its own axis.

In the model of inheritance of layers orientation the dependence of a diffraction pattern on the chiral indexes of layers allows determining the chiral indexes of multiwall nanotube (p_0, s_0) and further – the whole set of chiral indexes of nanotube's layers. The authors do not consider a model of inheritance as the only, but assume that this model is prevailing. Also the model in which in (2) the chiral indexes of a layer (p_m,s_m) are determined not as the nearest integers, but by rounding off in a direction of increase is possible. It will mean that the radiuses of the next layers can not differ by the value smaller than d. It is obvious that in this case the dependences of positions and forms of multiwall nanotube's reflexes on chiral indexes, specified in the article, will amplify.

The essential point of the proposed as the first approach mathematical apparatus is taking into account only those members of expanding of diffraction amplitude into a series of cylindrical waves (series over q) which make the maximum contribution. This does not cause doubts when the selection rule arises from the lattice sum along a nanotube's axis (over n), as the number of addendums in this sum is rather great and is well approximated by δ-function. However the number of addendums in the azimuthal lattice sum (over v) is not so great, therefore an appreciable contribution can be made not only by the chosen member of a series but also by members with q-1 and q+1.

It can result in the occurrence of a set of diffraction effects more fine than the considered above. For example, there can be some angular dependence (on φ^*) intensity of all reflexes of a singlewall chiral nanotube, except for reflexes 00*l*. Also there can be some deviations of the form of the given calculated diffraction patterns. The analysis of these effects will be continued further.

The proposed mathematical apparatus simulation of diffraction by chiral nanotubes is more general than the earlier published one [5] for the case of circular nanotubes and contains it as a special case at $s_m = 0$. Really, in this case values (2) transform into

$$w_m = bp_m, \; p_m = \frac{2pr_m}{b},$$

$$r_{mj} = r_m + x_j, \; a_{1m} = \frac{2p}{p_m},$$

$$b_{1m} = a_{2m} = 0, \quad b_{2m} = a,$$

$$g_{1mj} = \frac{2p\,y_j}{bp_m} + e_m, \quad g_{2mj} = z_j,$$

and
$$F_{mj}(z^*) = f_j \exp\left(2piz^* z_j\right)\exp\left(2piz^* \Delta z_m\right) \qquad (27)$$

Then the sums over v in amplitude (5) become trivial and there will be only one condition (7), which gives: $z^* = h/a$ – the equations of layer planes, on which the strong reflexes of circular nanotube are located. The substitution of the obtained values in (5) gives the corresponding expression from [5] for amplitude of circular nanotube's strong reflexes.

The diffuse reflexes of chiral nanotube, as against the circular one, are split in pairs, whose intensities are given by the expressions (21) and (22). Hence, the sum of these expressions corresponds to the case of circular nanotube. If we use values (27) the conditions of maximum of expressions (20) give: $q = kp_m$ and $z^* = h/a$ – the equations of layer planes, on which all, including the diffuse ones, reflexes of circular nanotube are located. Then both in (21) and (22) there remains only one addendum, corresponding to this value q, and their sum will give expression for amplitude of diffuse reflexes from circular nanotube, given in [5]. The expression (24) becomes unacceptable, as the condition of strong reflexes ($k = 0$) gives: $q = 0$, while in amplitude (6), from which (24) is deduced, $q \geq 1$ by definition.

In the following article of this series the quantitative theory of diffraction by spiral nanotubes of arbitrary chemical composition will be proposed.

References

[1] Whittaker E.: Acta Cryst.,1955, **8**, 725.
[2] Nasyrov I., Pashin D., Khalitov Z. and Valeeva D.: Scientific Israel – Technol. Adv., 2010, **12**, 63.
[3] Lambin Ph. and Lucas A.: Phys. Rev. B, 1997, **56**, 3571.
[4] Qin L.: Phys. Chem. Chem. Phys., 2007, **9**, 31.
[5] Figovsky O., Nasyrov I., Pashin D. *et al.*: Chem. & Chem. Techn., 2012, **6**, 43.
[6] Gricaenko G., Zviagin B., Boiarskaia R. *et al.*: Metody Elektronnoi Microskopii Mineralov. Nauka, Moskwa 1969.
[7] Galimov E. and Khalitov Z.: Modelirovanie Difrakcii Nanotrubkami. Kazan State Techn. Univ., Kazan 2007.
[8] Krinary G. and Halitov Z.: Proc. the First EPDIC. Munich 1991, 191.
[9] Whittaker E.: Acta Cryst., 1954, **7**, 827.

МОДЕЛЮВАННЯ ДИФРАКЦІЇ ХІРАЛЬНИМИ НАНОТРУБКАМИ ДОВІЛЬНОГО СКЛАДУ

Анотація. *Запропоновано кількісну теорію дифракції за допомогою окремих хіральних нанотрубок довільного хімічного складу. Досліджено вплив псевдоортогональності та залежність дифракції від азимутальної впорядкованості. Наведено розрахункові дифрактограми для випадку електронної мікродифракції окремими хризотиловими нанотрубками.*

Ключові слова: *нанотрубки, хіральні нанотрубки, індекси хіральності.*